Gaseous microflow modeling using the Fokker-Planck equation

S. K. Singh,[1] Chakradhar Thantanapally,[2] and Santosh Ansumali[1,*]
[1]*Engineering Mechanics Unit, Jawaharlal Nehru Centre for Advanced Scientific Research, Jakkur, Bangalore 560064, India*
[2]*SankhyaSutra Labs Pvt. Ltd., Bangalore 560064, India*
(Received 2 August 2015; published 27 December 2016)

We present a comparative study of gaseous microflow systems using the recently introduced Fokker-Planck approach and other methods such as: direct simulation Monte Carlo, lattice Boltzmann, and variational solution of Boltzmann-BGK. We show that this Fokker-Plank approach performs efficiently at intermediate values of Knudsen number, a region where direct simulation Monte Carlo becomes expensive and lattice Boltzmann becomes inaccurate. We also investigate the effectiveness of a recently proposed Fokker-Planck model in simulations of heat transfer, as a function of relevant parameters such as the Prandtl, Knudsen numbers. Furthermore, we present simulation of shock wave as a function of Mach number in transonic regime. Our results suggest that the performance of the Fokker-Planck approach is superior to that of the other methods in transition regime for rarefied gas flow and transonic regime for shock wave.

DOI: 10.1103/PhysRevE.94.063307

I. INTRODUCTION

The fluid dynamics of gases at the micrometer scale has attracted a lot of attention in recent years due to engineering applications in areas such as microelectromechanical systems, shale gas transport, and fuel cells [1–5]. In these setups, the physical length scale is of the order of the mean free path and thus continuum approximation starts to break down. Due to strong departure from equilibrium behavior in these setups Navier-Stokes-Fourier (NSF) equations are no longer valid. In this regime, the dilute gas dynamics is well described by the Boltzmann equation [6,7]. Due to the complexity of the Boltzmann collision term, one often resorts to numerical simulation using the direct simulation Monte Carlo (DSMC) method [1,8–10]. However, due to low Mach number (Ma) and low (but finite) Knudsen number (Kn) regime, large statistical fluctuations make efficient numerical simulations using DSMC quite expensive [1]. In order to reduce computational costs, simplified collision mechanism and discrete models such as Lattice Boltzmann (LB) discrete velocity models [4,11–26] are often used. Theses discrete velocity models were also used to get analytical solutions for canonical flows in microflow regime [15,23,26]. Out of all these approaches, LB has emerged as a viable methodology for microflow simulations at low mach number and moderate Knudsen number. Due to computational efficiency of LB, these methods were often used to get numerical solutions in nontrivial microflow setups as well [4,5,26]. These results show that lower-order LB models are limited to $\mathrm{Kn} < 0.1$ [20], whereas higher-order LB models provide correct results up to $\mathrm{Kn} < 0.25$ in isothermal setups [15,20].

Ideally, one would like to have accuracy of DSMC method with computational efficiency of mesoscale methods such as LB. In this context, it was recently pointed out that another possible computationally attractive option is to work with the Fokker-Planck (FP) collision model [27–29]. The computational motivation behind this approach is that, unlike DSMC, collision dynamics for FP model is much simpler and can be mapped to computationally efficient Langevin dynamics [30,31]. The basic model in this approach is the FP collision model proposed by Lebowitz *et al.* [32], where the Boltzmann collision operator was replaced by a diffusive dynamics in velocity space. Though this model has correct hydrodynamic limit [32], like BGK collision model [33], this model also leads to a wrong value of the Prandtl number (Pr). Unlike, Boltzmann equation, which predicts the Prandtl number of monatomic gas to be $\mathrm{Pr} = 2/3$, Lebowitz *et al.*'s [32] FP model predicts $\mathrm{Pr} = 3/2$ and the BGK model predicts $\mathrm{Pr} = 1$. An alternate modification to the original FP model [32] is proposed in Ref. [34], where the Prandtl number appears as a free parameter in the kinetic model. It was shown that this approach, when coupled with the FP approach, leads to a simple but quite accurate model with flexible Prandtl number (Pr) and a valid H-theorem. In the present study, we explore the effectiveness of this approach by simulating various canonical flows such as: Couette flow, Poiseuille flow, normal shock wave, and heat transfer between parallel heated plates over a wide range of Kn and contrasting the result with known numerical (DSMC) and analytical solutions of the Boltzmann BGK equation for canonical flows [15,20,35–39].

The present work is arranged as follows: In Sec. II, the Boltzmann equation, BGK model, and phenomenological FP model with its properties are discussed in detail. In Sec. III, Langevin equations corresponding to the FP equation are provided and solution algorithm is discussed. In Sec. IV, we describe the existing analytical and numerical solutions of the Couette flow, Poiseuille flow, heat flow between two infinitely long parallel plates, and normal shock tests. Furthermore, we present simulation results for these flows via present FP model and compare with existing solutions obtained using analytical, DSMC, LB, etc. In Sec. V, conclusion of the study is presented and effectiveness of this model is discussed in brief.

II. BOLTZMANN EQUATION AND FOKKER-PLANCK MODEL

The Boltzmann equation provides a quantitatively correct dynamics of the dilute gas even when the gas is far away from equilibrium. In this description, the state of the gas at any location $\mathbf{x} \in \mathcal{R}^3$ and time $t \geqslant 0$ is described in terms of the single-particle distribution function $f(\mathbf{x},\mathbf{c},t) \geqslant 0$, where $\mathbf{c} \in \mathcal{R}^3$ is the molecular velocity. $f(\mathbf{x},\mathbf{c},t)d\mathbf{x}d\mathbf{c}$ is the probability

*ansumali@jncasr.ac.in

of finding a particle centered at the point $(\mathbf{x},\mathbf{c})$ in infinitesimal volume $d\mathbf{x}d\mathbf{c}$. In order to define macroscopic quantities, it is convenient to first define inner product:

$$\langle \phi_1(\mathbf{c}),\phi_2(\mathbf{c})\rangle = \int_{-\infty}^{\infty}\int_{-\infty}^{\infty}\int_{-\infty}^{\infty} d\mathbf{c}\phi_1\,\phi_2, \tag{1}$$

where $\phi(\mathbf{c})$ is a polynomial of molecular velocity. As the description is that rarefied gas, the equation of state in this description is that of an ideal gas and the Temperature T of the gas is defined in terms of the internal energy e and mass density ρ as $e = 3\,\rho k_{\mathrm{B}}T/(2m)$, where k_{B} is the Boltzmann constant and m is the mass of a gaseous particle.

The macroscopic quantities such as mass density ρ, momentum density $j = \rho\mathbf{u}$ with u as mean velocity and energy density $E = \rho\mathbf{u}^2/2 + e$ are obtained as lower-order moments of f defined by the following relation:

$$\rho = \langle 1, f\rangle, \qquad \rho\mathbf{u} = \langle \mathbf{c}, f\rangle, \qquad e = \left\langle \frac{\xi^2}{2}, f\right\rangle, \tag{2}$$

where $\boldsymbol{\xi} = \mathbf{c} - \mathbf{u}$ is the peculiar velocity. The stress tensor $\sigma_{\alpha\beta}$ and heat flux q_α are

$$\sigma_{\alpha\beta} = \langle \overline{\xi_\alpha\xi_\beta}\rangle \text{ and } q_\alpha = \left\langle \frac{\xi_\alpha\xi^2}{2}\right\rangle, \tag{3}$$

where for any second-order tensor $A_{\alpha\beta}$, its traceless part $\overline{A}_{\alpha\beta} = (A_{\alpha\beta} + A_{\beta\alpha})/2 - A_{\gamma\gamma}/D\delta_{\alpha\beta}$. Similarly, the flux of stress tensor is related to the traceless part of third-order moment

$$Q_{\alpha\beta\gamma} = \int d\mathbf{c} f\Big[\xi_\alpha\xi_\beta\xi_\gamma - \frac{1}{D+2}(\xi^2\xi_\alpha\delta_{\beta\gamma} + \xi^2\xi_\beta\delta_{\gamma\alpha} + \xi^2\xi_\gamma\delta_{\alpha\beta})\Big]. \tag{4}$$

The time evolution of single-particle distribution f as governed by the Boltzmann equation [6,7] is

$$\partial_t f + c_\alpha\partial_\alpha f = \Omega^{\mathrm{B}}(f,f), \tag{5}$$

where Boltzmann collision operator Ω^{B}, a bilinear function of f. Due to the complexity of the Boltzmann collision term for many applications, one resorts to simplified collision models [7]. The simplest approximation of Boltzmann collision is given by Bhatnagar, Gross, and Krook (BGK) [33], where it is assumed that the collision dynamics can be replaced by relaxation toward the Maxwell-Boltzmann distribution,

$$f^{\mathrm{MB}} = \rho\left(\frac{m}{2\pi k_B T}\right)^{3/2}\exp\left(-\frac{m\xi^2}{2k_B T}\right), \tag{6}$$

with single relaxation time τ as the mean free time. The explicit form of BGK collision model is

$$\Omega^{\mathrm{BGK}} = \frac{1}{\tau}(f^{\mathrm{MB}} - f). \tag{7}$$

This model preserves almost all of the qualitative features of the Boltzmann collision term [6,7]. The simplicity of the form and having qualitative correct features of the Boltzmann equation make BGK quite suitable for understanding of phenomena far from equilibrium [7,40] and this model is routinely used for analytical as well as numerical investigations of gas flows [15,16,20,35,36,38]. However, a quantitative comparison with Boltzmann dynamics is not possible when heat transfer is also under consideration. As the basic assumption behind BGK approximation is that the relaxation of all higher-order moments toward their Maxwell-Boltzmann value happens with the same rate of relaxation, Prandtl number (Pr = 1) for monatomic gas flow is wrongly predicted by the model. This defect was removed by more refined model such as Ellipsoidal-BGK model [41].

Lebowitz's *et al.* [32] introduced an alternate way to simplify collision dynamics, which introduces a diffusion term in the velocity space to model the Boltzmann collision term. Unlike the BGK model, this model was largely ignored in gas dynamics applications. Recently, there is a renewed interest in this model due to its potential utility as an efficient numerical tool. A series of works have shown the feasibility of this model via Langevin dynamics [27–29,42–46]. However, this model predicts Prandtl number Pr = 3/2 for monatomic gases, which does not match with the prediction of Boltzmann equation (Pr = 2/3). To make FP model a better approximation to the Boltzmann equation, Gorji *et al.* [29] introduced a modified FP approximation with nonlinear drift term to correct the Prandtl number (Pr = 2/3). Afterwards, to introduce Prandtl number as a free parameter in the model, an alternate modification of the original FP model was proposed in Ref. [34]. In this model, following Ref. [47], an additional contribution to the advective term of the Boltzmann equation was added. In the free flight term of the Boltzmann equation, they used apparent streaming velocity $\hat{c}_\alpha$ [47] as

$$\hat{c}_\alpha = c_\alpha - \frac{\tau_{\mathrm{FP}}}{2}\lambda^q\left(\xi^2 - \frac{3k_{\mathrm{B}}T}{m}\right)\partial_\alpha \ln T + \chi(\rho)\xi_\alpha, \tag{8}$$

with λ^q is a positive constant related to the Prandtl number and τ_{FP} as the relaxation time associated with the FP model and $\chi(\rho)$ is the compressibility factor, relevant for corrections due to nonidea gas behavior. In present work we are interested in rarefied gas behavior only, so compressibility $\chi = 0$ is set in present work. The physical motivation behind this model can be easily understood by considering the motion of a tagged particle. According to Eq. (8), if the tagged particle finds itself in nonhomogenous temperature field, it gets a correction in velocity depending on local temperature gradient. Using this apparent streaming velocity, the FP model [32] was modified as

$$\partial_t f + \partial_\alpha[\hat{c}_\alpha f] = \Omega^{\mathrm{FP}}, \tag{9}$$

where Ω^{FP} is the FP collision operator, defined as

$$\Omega^{\mathrm{FP}} = \frac{1}{\tau_{\mathrm{FP}}}\partial_{c_\alpha}\left(\xi_\alpha f + \frac{k_B T}{m}\frac{\partial f}{\partial c_\alpha}\right). \tag{10}$$

This model assumes that the approach toward equilibrium (via collision process) can be well approximated by diffusion in the velocity space. The physical rationale is that many qualitative features of the binary collision (the Boltzmann dynamics) remains intact if we replace it with collision of a tagged molecule with a heat bath. This simplification of the collision mechanism leads to an $O(N)$ algorithm to simulate Boltzmann-type dynamics, which is $O(N^2)$. It needs to be remarked that although the correction to the advection velocity is orthogonal to the mass conservation in the present FP model, it gives finite contribution to the stresses. This is evident due

to the relation

$$\langle f(\hat{c}_\alpha - c_\alpha),1\rangle = 0, \quad \langle f(\hat{c}_\alpha - c_\alpha),c_\beta\rangle = -\tau_{\rm FP}\lambda^q q_\beta \partial_\alpha \ln T. \tag{11}$$

Similarly, the projection to the energy conservation by this correction term is

$$\langle f(\hat{c}_\alpha - c_\alpha),c^2\rangle = \left(-\frac{\tau_{FP}}{2}\lambda^q \partial_\alpha \ln T\right)\left(R' + \frac{6p^2}{\rho} + 4u_\beta q_\beta\right). \tag{12}$$

In this section, we briefly highlight some of the key features of this Boltzmann-Fokker-Planck dynamics.

(1) Collisional invariants: In this collision model too, the only invariants of the collision term are the mass, the momentum, and the energy. This is evident due to the following identity involving FP collision operator:

$$\langle \Omega^{\rm FP},\phi(\mathbf{c})\rangle = -\frac{1}{\tau_{\rm FP}}\int_{-\infty}^{\infty}\int_{-\infty}^{\infty}\int_{-\infty}^{\infty} d\mathbf{c}\left(\xi_\alpha f + \frac{k_B T}{m}\frac{\partial f}{\partial c_\alpha}\right)\frac{\partial \phi}{\partial c_\alpha}, \tag{13}$$

where surface terms have dropped out due to the fact that the distribution function attains zero value at infinity faster than any polynomial. This implies that for $\phi_0 = a_1 + \mathbf{a}_2\cdot\mathbf{c} + a_3\mathbf{c}^2$, we have

$$\langle \Omega^{\rm FP},\phi_0\rangle = -\frac{1}{\tau_{\rm FP}}\int_{-\infty}^{\infty}\int_{-\infty}^{\infty}\int_{-\infty}^{\infty} d\mathbf{c}\left(\xi_\alpha f + \frac{k_B T}{m}\frac{\partial f}{\partial c_\alpha}\right) \times (a_{2\alpha} + 2a_3 c_\alpha) = 0. \tag{14}$$

Thus, similar to the Boltzmann collision term or BGK collision term, the FP model also satisfies the condition $\langle \Omega^{\rm FP},\{1,\mathbf{c},\mathbf{c}^2\}\rangle = 0$.

(2) Conservation laws: The macroscopic conservation laws obtained from kinetic Eq. (9) by taking appropriate moment of the distribution function are

$$\begin{aligned} \partial_t \rho + \partial_\alpha j_\alpha &= 0,\\ \partial_t j_\alpha + \partial_\beta(\rho u_\alpha u_\beta + p\delta_{\alpha\beta}) + \partial_\beta \sigma^N_{\alpha\beta} &= 0,\\ \partial_t E + \partial_\alpha\big((E+p)u_\alpha + \sigma^N_{\alpha\gamma}u_\gamma\big) + \partial_\alpha q^N_\alpha &= 0, \end{aligned} \tag{15}$$

where $p\ (=\rho k_{\rm B}T/m)$ is the pressure term and the corrected stress $\sigma^N_{\alpha\beta}$ and corrected heat flux q^N_α as

$$\begin{aligned} \sigma^N_{\alpha\beta} &= \sigma_{\alpha\beta} - \tau_{\rm FP}\lambda^q\, q_\beta\, \partial_\alpha \ln T,\\ q^N_\alpha &= q_\alpha - \frac{3}{2}\rho\tau_{\rm FP}\left(\frac{k_{\rm B}T}{m}\right)^2\lambda^q\partial_\alpha \ln T - \frac{\tau_{\rm FP}}{4}\lambda^q R'\partial_\alpha \ln T, \end{aligned} \tag{16}$$

which has an additional contribution other than kinetic part $\sigma_{\alpha\beta}$ and q_α due to temperature gradient. Here, the form of conservation laws remain the same as macroscopic hydrodynamics. Thus, similar to Boltzmann dynamics, the present model also correctly predicts the correct macroscopic behavior.

(3) Maxwell-Boltzmann distribution: For this model, zero of collision term suggests

$$\frac{1}{\tau_{\rm FP}}\partial_{c_\alpha}\left(\xi_\alpha f + \frac{k_B T}{m}\frac{\partial f}{\partial c_\alpha}\right) = 0. \tag{17}$$

Integrating Eq. (17) with respect to the velocity space and using the fact that distribution function and its derivative attains the zero value at infinity, we have

$$\xi_\alpha f + \frac{k_B T}{m}\frac{\partial f}{\partial c_\alpha} = 0. \tag{18}$$

Solving Eq. (18), we get the Maxwell-Boltzmann distribution as a solution. Thus, similar to Boltzmann dynamics, the present model has Maxwell-Boltzmann distribution at equilibrium.

(4) *H* theorem: Like Boltzmann dynamics, the nonequilibrium generalization of the entropy is given by H function defined as $H = \int d\mathbf{c}(f\ln f - f)$. The evolution equation for H function using Eq. (9) is written as

$$\partial_t H + \partial_\alpha \int d\mathbf{c}\hat{c}_\alpha f(\ln f - 1) = \langle \Omega^{\rm FP}, \ln f\rangle = -\Xi, \tag{19}$$

where Ξ is the entropy production term and it is positive definite as

$$\Xi = \left(\frac{\tau_{\rm FP}}{2}\lambda^q\left(\frac{3\rho k_{\rm B}T}{m}\right)(\partial_\alpha \ln T)^2 + \left\{\int d\boldsymbol{\xi}\, f\left[\frac{\partial \ln\left(\frac{f}{f^{\rm MB}}\right)}{\partial \xi_\alpha}\right]^2\right\}\right) \geqslant 0, \tag{20}$$

where following identity was used to show positivity of the entropy production,

$$\int d\boldsymbol{\xi}\, f\left[\frac{\partial \ln\left(\frac{f}{f^{\rm MB}}\right)}{\partial \xi_\alpha}\right]^2 = -\frac{3\,\rho m}{k_{\rm B}T} + \int d\boldsymbol{\xi}\,\frac{1}{f}\frac{\partial f}{\partial \xi_\alpha}\frac{\partial f}{\partial \xi_\alpha}. \tag{21}$$

(5) Hydrodynamics and transport properties: For this FP model of the Boltzmann equation, the evolution equation for the higher-order moments like $\sigma_{\alpha\beta}$ and q_α are

$$\begin{aligned} &\partial_t\sigma_{\alpha\beta} + A_{\alpha\beta} + 2p\overline{\partial_\alpha u_\beta} - \frac{1}{2}\partial_k\left[\lambda^q\tau_{\rm FP}(\partial_k \ln T)\right.\\ &\left.\times\left(R_{\alpha\beta} - \frac{3k_BT}{m}\sigma_{\alpha\beta}\right)\right] - (\tau_{\rm FP}\lambda^q\partial_k \ln T)\overline{q_\beta\partial_k u_\alpha}\\ &= -\frac{2\sigma_{\alpha\beta}}{\tau_{\rm FP}}, \end{aligned} \tag{22}$$

where term $A_{\alpha\beta}$, which is nonzero only in the nonequilibrium condition, is given as

$$A_{\alpha\beta} = \partial_\gamma(\sigma_{\alpha\beta}u_\gamma) + 2\overline{\sigma_{\alpha\gamma}\partial_\gamma u_\beta} + \partial_\gamma Q_{\alpha\beta\gamma} + \frac{4}{D+2}\overline{\partial_\alpha q_\beta}. \tag{23}$$

Similarly, evolution equations for the heat flux q_α is

$$\partial_t q_\alpha + B_\alpha + \frac{(D+2)}{2} p\partial_\alpha \frac{p}{\rho} + \frac{2}{D+2}(q_\gamma \partial_\alpha u_\gamma + q_\alpha \partial_\beta u_\beta) - \frac{1}{4}\partial_k\left[\lambda^q \tau_{\rm FP}(\partial_k \ln T)\left(\Lambda_\alpha - 6\frac{p}{\rho}q_\alpha\right)\right]$$
$$-\frac{1}{4}(\tau_{\rm FP}\lambda^q \partial_\beta \ln T)\left(R' + \frac{6(p)^2}{\rho}\right)\partial_\beta u_\alpha - \frac{1}{4}(\tau_{\rm FP}\lambda^q \partial_\beta \ln T)\left(R_{\alpha k} + \frac{R'\delta_{\alpha k}}{D} + \frac{2p^2\delta_{\alpha k}}{\rho} - \frac{3p\sigma_{\alpha k}}{\rho}\right)\partial_\beta u_k = -\frac{3q_\alpha}{\tau_{\rm FP}}, \quad (24)$$

where term B_α, which is nonzero only in the nonequilibrium condition, is

$$B_\alpha = \partial_\beta\left(q_\alpha u_\beta + \frac{R_{\alpha\beta}}{2} + \frac{R'\delta_{\alpha\beta}}{2D}\right) + \frac{2}{D+2}(q_\gamma \partial_\alpha u_\gamma + q_\alpha \partial_\beta u_\beta) - \frac{\sigma_{\alpha\beta}\partial_\beta p}{\rho} + \frac{(D+4)}{D+2} q_\beta \partial_\beta u_\alpha$$
$$+ Q_{\alpha\beta\gamma}\partial_\beta u_\gamma - \frac{(D+2)p}{2\rho}\partial_\beta \sigma_{\alpha\beta} - \frac{\sigma_{\alpha\kappa}\partial_\beta \sigma_{\kappa\beta}}{\rho}, \quad (25)$$

with $R' = \int d\mathbf{c} f \xi^2 \xi^2 - (15p^2/\rho)$, $R_{\alpha\beta} = \int d\mathbf{c} f \xi^2 \overline{\xi_\alpha \xi_\beta}$. and $\Lambda_\alpha = \int d\mathbf{c} f \xi^2 \xi^2 \xi_\alpha$. Here, it is evident from evolution equation for stress and heat flux that the moment chain is not closed. However, in the limit of Knudsen number going to zero, the dynamics of higher-order moments get decoupled with the dynamics of lower-order moments. In order to derive the transport coefficients, we analyze the hydrodynamic limit of the FP model by applying the Chapman-Enskog expansion procedure on Eqs. (22) and (24) (here the distribution function and time derivative of nonconserved quantity are expanded in terms of $\tau_{\rm FP}$); finally, we have

$$\sigma_{\alpha\beta} = -\tau_{\rm FP} p \overline{\partial_\alpha u_\beta}, \quad q_\alpha = -\tau_{\rm FP}\frac{D+2}{6} p\partial_\alpha \frac{p}{\rho}. \quad (26)$$

Using Eqs. (26) and (16) while retaining only first-order terms in $\tau_{\rm FP}$, we obtain

$$\sigma^N_{\alpha\beta} = -2\left(\frac{\tau_{\rm FP} p}{2}\right)\overline{\partial_\alpha u_\beta},$$
$$q^N_\alpha = -\tau_{\rm FP}\left[\frac{D+2}{6} p\partial_\alpha \frac{p}{\rho} + \frac{3}{2}\rho\left(\frac{k_{\rm B}}{m}\right)^2 T\lambda^q \partial_\alpha T\right]. \quad (27)$$

Thus, we have viscosity coefficient (μ) and heat conductivity (κ) as

$$\mu = \frac{\tau_{\rm FP} p}{2},$$
$$\kappa = \tau_{\rm FP}\left[\frac{D+2}{6}\frac{k_{\rm B}}{m} p + \frac{3}{2}\rho\left(\frac{k_{\rm B}}{m}\right)^2 T\lambda^q\right], \quad (28)$$

which implies that the Prandtl number is

$$\Pr = \frac{3C_p}{2C_p + 9\lambda^q(k_{\rm B}/m)}. \quad (29)$$

Equation (29) allows us to choose the Prandtl number independently in interval $(0, \frac{3}{2}]$.

It is evident that Lebowitz's *et al.* [32] model is a special case, which can be obtained via setting $\lambda^q = 0$. Thus, Fokker-Planck model considered in the present work provides a convenient phenomenological description of gaseous flow at kinetic level. Unlike BGK model, present model can be discretized using particle methods (similar to DSMC) in a straight-forward manner. The next section will describe one such discretization strategy.

III. LANGEVIN EQUATION AND SOLUTION ALGORITHM

The FP model presented above [Eq. (9)] can be transformed into equivalent Langevin equation for particles [48]. In the present case, for an ensemble of gaseous molecules whose states (x_α, c_α), the equivalent Langevin equation is

$$dx_\alpha = c_\alpha dt - \frac{\tau_{\rm FP}}{2}\lambda^q(\partial_\alpha \ln T)\left(\xi^2 - D\frac{k_B T}{m}\right)dt,$$
$$dc_\alpha = -\frac{\xi_\alpha}{\tau_{\rm FP}}dt + \sqrt{2\frac{k_{\rm B}T}{m}}dW_\alpha, \quad (30)$$

where $W(t)$ with $dW(t) = W(t+dt) - W(t)$ is the standard Weiner process, which is a rapidly changing random force with mean and variance as

$$\langle dW_\alpha\rangle = 0, \quad \langle dW_\alpha dW_\beta\rangle = dt\delta_{\alpha\beta}. \quad (31)$$

Thus, the detailed binary collision description is approximated by a random collision with a heat bath in the model.

These stochastic differential equations of Langevin type can be solved quite efficiently. To solve the Langevin equations [Eq. (30)], the stochastic version of the Verlet algorithm [49] is applied. The stochastic Verlet scheme for the present model is

$$x^{(1)}_\alpha = x_\alpha + \frac{1}{2}\left[c_\alpha(t) - \frac{\tau_{\rm FP}}{2}\lambda^q(\partial_\alpha \ln T)\left(\xi^2 - D\frac{k_B T}{m}\right)\right]\Delta t,$$
$$c_\alpha(t+\Delta t) = c_\alpha(t) - \frac{\vartheta}{1+\vartheta/2}[c_\alpha(t) - u_\alpha] + \frac{\sqrt{2\frac{k_{\rm B}T}{m}\vartheta}}{1+\vartheta/2}\phi_t,$$
$$x_\alpha(t+\Delta t) = x^{(1)}_\alpha + \frac{1}{2}\left[c_\alpha(t+\Delta t) - \frac{\tau_{\rm FP}}{2}\lambda^q(\partial_\alpha \ln T)\left(\xi^2 - D\frac{k_B T}{m}\right)\right]\Delta t, \quad (32)$$

where $\vartheta = \frac{\Delta t}{\tau_{\rm FP}}$ and ϕ_t is normal random number generator with mean 0 and variance 1. This scheme works efficiently for small time step, i.e., $\vartheta < 0.01$. Temperature gradient term in Eq. (32) can be easily evaluated using Eq. (26), then we have

$$x_\alpha^{(1)} = x_\alpha + \frac{1}{2}\Bigg[c_\alpha(t) + \frac{27\lambda^q \rho q_\alpha}{4(D+2)e^2}\left(\xi^2 - D\frac{k_B T}{m}\right)\Bigg]\Delta t,$$

$$c_\alpha(t+\Delta t) = c_\alpha(t) - \frac{\vartheta}{1+\vartheta/2}[c_\alpha(t) - u_\alpha] + \frac{\sqrt{2\frac{k_B T}{m}\vartheta}}{1+\vartheta/2}\phi_t,$$

$$x_\alpha(t+\Delta t) = x_\alpha^{(1)} + \frac{1}{2}\Bigg[c_\alpha(t+\Delta t) + \frac{27\lambda^q \rho q_\alpha}{4(D+2)e^2}\left(\xi^2 - D\frac{k_B T}{m}\right)\Bigg]\Delta t. \quad (33)$$

In particular, $\lambda^q = 5/18$ for BGK model (Pr = 1).

For actual implementation, similar to DSMC, physical domain can be partitioned into cells of size similar to mean free path. As FP is stochastic like DSMC, required physical quantities are calculated as averages. For example, physical quantities like mass density (ρ), momentum density (ρu), and energy (**e**) density are given by

$$\rho_i = \frac{1}{V_{\rm cell}}\sum_i m, \quad \rho_i u_i = \frac{1}{V_{\rm cell}}\sum_i m c_i, \quad \mathbf{e}_i = \frac{1}{V_{\rm cell}}\sum_i m|c_i|^2, \quad (34)$$

where summation is taken over the ith cell, and m and $V_{\rm cell}$ are mass of particle and volume of computational cell, respectively. We need sufficient number of particles in each cell to reduce statistical fluctuations about the average.

The wall boundary condition can be implemented using diffusive wall approximation (regularly used for DSMC), where it is assumed that any particle hitting the wall emerges in a random direction with conditions corresponding to wall equilibrium. The physical picture behind this model is that a particle hitting the wall get absorbed in the wall and undergoes multiple collisions before reemerging in the fluid [50]. Thus, a particle emerging from the wall has no memory of its initial velocity and acquires Maxwell-Boltzmann distribution corresponding to the wall temperature T_w and wall velocity $\mathbf{u}_w$. The component normal to the wall $v_\perp$ have a distribution

$$f(v_\perp) = \frac{m}{k_{\rm B} T_w} v_\perp \exp\left(-\frac{m v_\perp^2}{2k_{\rm B} T_w}\right), \quad (35)$$

while each parallel component will have distribution

$$f(v_\parallel) = \sqrt{\frac{m}{2\pi k_{\rm B} T_w}}\exp\left(-\frac{m(v_\parallel - u_w)^2}{2k_{\rm B} T_w}\right). \quad (36)$$

In actual implementation, the biased Maxwellian distribution in normal direction can be achieved by introducing a variable transformation

$$r_u = \exp\left(-\frac{m v_\perp^2}{2k_{\rm B} T_w}\right). \quad (37)$$

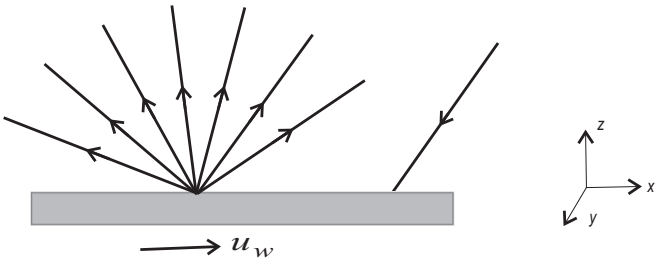

FIG. 1. Geometrical representation diffusive boundary condition.

It is straight forward to verify that if r_u is a uniformly distributed random number in (0,1) then $v_\perp$ will be distributed according to Eq. (35). The parallel component can be generated via standard Box-Muller transform [31]. As a specific example, as shown in Fig. 1, we consider wall normal to be in z direction and wall to be moving in x direction with velocity u_w. In this case the three components of the velocity of a particle emerging from wall can be written as

$$v_x = \sqrt{\frac{kT_w}{m}}r + u_w, \quad v_y = \sqrt{\frac{kT_w}{m}}r', \quad v_z = \sqrt{-\frac{2kT_w}{m}\ln r_u}, \quad (38)$$

where r_u is uniformly distributed random numbers in (0,1) and, r and r' are the Gaussian random numbers distributed with mean zero and variance one, respectively.

Finally, for engineering applications, one needs to specify inlet and outlet boundary conditions too. In the present FP framework, we work with local one-dimensional approach regularly used for Euler equations [51]. First, we assume that near inlet and outlet distribution is well approximated by Maxwell-Boltzmann distribution. The assumption of Maxwell-Boltzmann and one dimensionality of the flow near boundary allow us to use characteristic analysis of the Euler equations [51], which gives characteristic velocities as $\lambda_1 = u - c, \lambda_5 = u + c, \lambda_2 = \lambda_3 = \lambda_4 = u$, and $c = \frac{\gamma p}{\rho}$, is the speed of sound with γ as the adiabatic exponent. The amplitudes of characteristic waves L_i's in terms of the characteristic velocities are

$$L_1 = \lambda_1\left(\frac{\partial p}{\partial x} - \rho c\frac{\partial u}{\partial x}\right),$$
$$L_2 = \lambda_2\left(c^2\frac{\partial \rho}{\partial x} - \frac{\partial p}{\partial x}\right),$$
$$L_3 = \lambda_3\frac{\partial v}{\partial x},$$
$$L_4 = \lambda_4\frac{\partial w}{\partial x},$$
$$L_5 = \lambda_5\left(\frac{\partial p}{\partial x} + \rho c\frac{\partial u}{\partial x}\right). \quad (39)$$

The local one-dimensional inviscid (LODI) analysis is used to calculate the outlet boundary conditions. In this case the problem is one-dimensional, which makes it one-dimensional

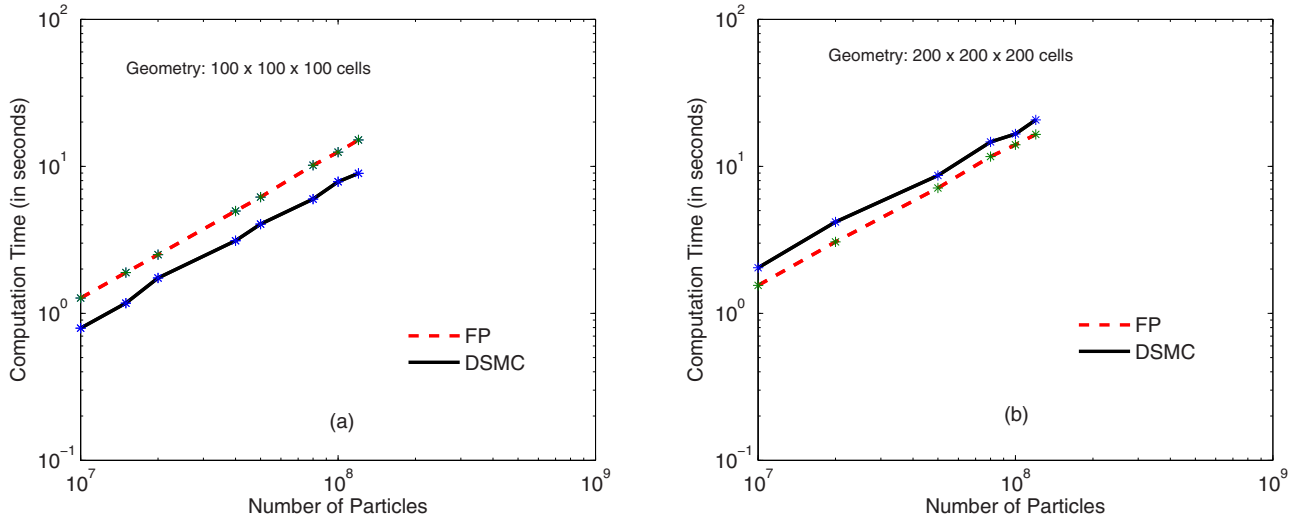

FIG. 2. Computation time as a function of numbers of particles for Fokker-Planck and DSMC (SPARTA).

globally as well. The LODI system in primitive variables is

$$\begin{aligned}
\frac{\partial \rho}{\partial t} + \frac{1}{c^2}\left[L_2 + \frac{1}{2}(L_5 + L_1)\right] &= 0,\\
\frac{\partial p}{\partial t} + \frac{1}{2}(L_5 + L_1) &= 0,\\
\frac{\partial u_1}{\partial t} + \frac{1}{2\rho c}(L_5 - L_1) &= 0,\\
\frac{\partial u_2}{\partial t} + L_3 &= 0,\\
\frac{\partial u_3}{\partial t} + L_4 &= 0.
\end{aligned} \tag{40}$$

In this approach, we used a supersonic inlet condition on the left boundary and a subsonic outlet condition on the right boundary according to Refs. [51,52]. All the variables (ρ, u, T) are imposed on the left boundary, as all the characteristics move into the interior of the domain for a supersonic inlet. For a subsonic outlet, we impose only pressure, as there is only one characteristic moving into the domain from outside, and the rest are calculated from the neighboring boundary cells according to Refs. [51,52]. Since we impose a steady pressure at the outlet, the LODI relation for pressure suggests that

$$L_1 = -L_5. \tag{41}$$

The rest of the L_i's are obtained from the interior of the domain using Eq. (39). We used a one-sided finite difference to calculate the spatial derivatives. All the variables except pressure are estimated from Eq. (40) to get their values at the next time step. As the density is proportional to the number of particles in a cell, additional particles are introduced and removed in the boundary cells according to the required density. The boundary cells are completely reinitialized uniformly in space and with Maxwellian distribution in velocity, pertaining to the values obtained at respective boundaries.

As discussed earlier, for rarefied gas flow the most widely used methodology is DSMC. The standard DSMC without making any approximation is $O(N^2)$ algorithm, with N being number of particles in a cell [50]. The algorithm is $O(N^2)$ due to the need of finding maximum relative velocity in every cell. However, DSMC algorithm can be modified into $O(N)$ alternate via approximating velocity maximum in a cell globally [50]. There are many highly optimized implementations of DSMC available in the literature. In order to compare speed between our FP algorithm and DSMC, we choose recently developed SPARTA framework for DSMC [53,54].

In the present algorithm, the binary collision is approximated by a Gaussian random noise. This simplification of the collision mechanism leads to an inherently $O(N)$ algorithm to simulate Boltzmann type dynamics. Both DSMC and FP approaches have their own strength and weaknesses. While, $O(N)$ version of DSMC collision is faster than FP due to the fact that it does not require Gaussian random number which involves significant amount of mathematical function calls such as logarithm. On the other hand, FP collision does not involve collision pairs, so collision implementation does not require sorting step. Thus, one would expect that DSMC is faster for smaller system size, whereas FP should become more efficient as system size increases.

In Fig. 2, FP algorithm and an $O(N)$ implementation of DSMC using SPARTA framework are contrasted for two different system sizes. As expected, DSMC is faster for smaller system size and FP is more efficient option for larger system size. Thus, present FP scheme is a potentially attractive $O(N)$ alternate to DSMC. Here, we would like to mention that it is just speed comparison of both the algorithms (not related with the convergence of result). Also, it is important to mention that all physical results simulated using FP algorithm (shown in next section) are contrasted only with results obtained by using basic $O(N^2)$ version of standard DSMC [50].

IV. BENCHMARKING FOR CANONICAL FLOWS

In order to show usefulness of the Fokker-Planck and Langevin approach, we shall consider a number of canonical set-ups of microflow. We restrict our attention to the set-up

of Couette flow, Poiseuille flow, heat transfer between parallel plates, and normal shock wave.

A. Couette flow

In Couette flow setup, steady flow is confined between two infinitely long parallel plates, which are moving with respect to each other. The lower and upper plates are kept at $x = -L/2$ and $x = L/2$, moving with velocity U_1 and U_2, respectively. The relative motion of both parallel plates generates a shear force, which is responsible for the motion of fluid. This setup is extensively studied via various analytical and numerical approaches [15,35–37]. Using BGK approximation, Willis [35] formulated this flow problem in terms of integral equation and solved using Wiener-Hopf technique. Later, Cercignani and coworkers [36] solved this integral equation formulation using a variational approach. Recently, it was recognized that discrete velocity model associated with the lattice Boltzmann model leads to a finite moment chain and explicit specification of the boundary condition in terms of these moment [15]. Using this moment chain for various lattice Boltzmann based discrete velocity models analytical solutions were obtained [15,20]. Later, these boundary value problems were also solved using the regularized-13 equations [37]. Based on these results, it can be said that the velocity profile in this setup is well approximated by an expression of the form (see Refs. [15,20,37])

$$u(y) = \frac{U_1 + U_2}{2} + \frac{1}{\Theta}\frac{y}{L}(U_2 - U_1) + \frac{1}{Z}(U_2 - U_1)\sinh\left(\frac{y}{c_1 \mathrm{Kn}\, L}\right), \tag{42}$$

where Θ, Z, and c_1 are the appropriate model dependent constants. Here, we have defined Knudsen number as $\mathrm{Kn} = (\tau_{\mathrm{FP}}/\mathrm{L})\sqrt{(\mathrm{k_B T})/2\mathrm{m}} = (\tau/\mathrm{L})\sqrt{(2\mathrm{k_B T})/\mathrm{m}}$, where L is the gap between the parallel plates. This allows us to write difference between nondimensional velocity gradient with its continuum value at the center-line (say, Y),

$$Y = 1 - \frac{1}{(U_2 - U_1)}\frac{\partial u_x}{\partial(y/L)}\bigg|_{y=0} = \frac{c_1 Z\mathrm{Kn}(\Theta - 1) - \Theta}{c_1 Z\mathrm{Kn}\Theta}, \tag{43}$$

and dimensionless velocity slip (S) at wall is given by

$$S = \frac{U_2 - U_1}{U_{\mathrm{wall}}}\left[\frac{1}{2} - \frac{1}{2\Theta} - \frac{1}{Z}\sinh\left(\frac{1}{2c_1\mathrm{Kn}}\right)\right]. \tag{44}$$

It has be shown that many higher-order LB models and R13 model are able to reproduce profiles suggested by Eq. (42) [15,20,37]. We choose to work with the LB model, which shows very good agreement with the true Boltzmann dynamics for the given setup. Following Ref. [15], for $D2Q16$ LB model, $c_1 = \sqrt{3/2}$ and values of Θ and Z are given as

$$\Theta = 1 + \frac{\sqrt{6}\mathrm{Kn}\left[3.076\sinh\left(\frac{1}{\sqrt{6}\mathrm{Kn}}\right) + 2\cosh\left(\frac{1}{\sqrt{6}\mathrm{Kn}}\right)\right]}{3.076\cosh\left(\frac{1}{\sqrt{6}\mathrm{Kn}}\right) + 2\sqrt{3}\sinh\left(\frac{1}{\sqrt{6}\mathrm{Kn}}\right)}, \tag{45}$$

$$Z = \frac{18.456(3.076\mathrm{Kn} + \sqrt{2})\sinh\left(\frac{1}{\sqrt{6}\mathrm{Kn}}\right) + 3.076(12\mathrm{Kn} + 7.53463)\cosh\left(\frac{1}{\sqrt{6}\mathrm{Kn}}\right)}{12\mathrm{Kn}}. \tag{46}$$

Similarly dimensionless shear stress (σ_{xy}) has the following form:

$$\sigma_{xy} = \frac{\left(\Upsilon_1 \coth\left(\frac{\Upsilon_2}{\mathrm{Kn}}\right) + \Upsilon_3\right)\mathrm{Kn}}{(\Upsilon_4 + \Upsilon_5\mathrm{Kn})\coth\left(\frac{\Upsilon_2}{\mathrm{Kn}}\right) + (\Upsilon_6 + \Upsilon_7\mathrm{Kn})}, \tag{47}$$

where $\Upsilon_1, \Upsilon_2 \ldots$ and Υ_7 are the appropriate model dependent constants [15,20,37].

To simulate the Couette flow using FP approach, we considered a computational zone of $200 \times 4 \times 4$ cells and each cell contains 500 gaseous particles, with initial density as $\rho_0 = 1$. Diffusive boundary condition was applied on moving walls and periodic boundary condition was used in the remaining directions (for details, see Ref. [50]). For low Kn simulation, the magnitude of ϑ is restricted to $\vartheta < 0.01$ due to stability constraints. Simulations for different values of Kn in transitional regime have been performed and compared with existing standard results for three important physical quantities related to Couette flow, i.e., shear stress, difference between centerline velocity gradient and its continuum value (based on NSF) and velocity slip at the wall. It is evident from the Fig. 3 (for shear stress) that FP approximation works quite well. Like Boltzmann-BGK, effective shear stress converges to 1 as $\mathrm{Kn} \to \infty$ for the modified FP approximation. Yet another important measure for departure from hydrodynamic behavior is difference between centerline velocity gradient and its continuum value (based on NSF). This quantity is evaluated via direct simulation using FP approach and compared with results obtained via Boltzmann-BGK-based method [35], DSMC method [15], and lattice Boltzmann method [20] for different

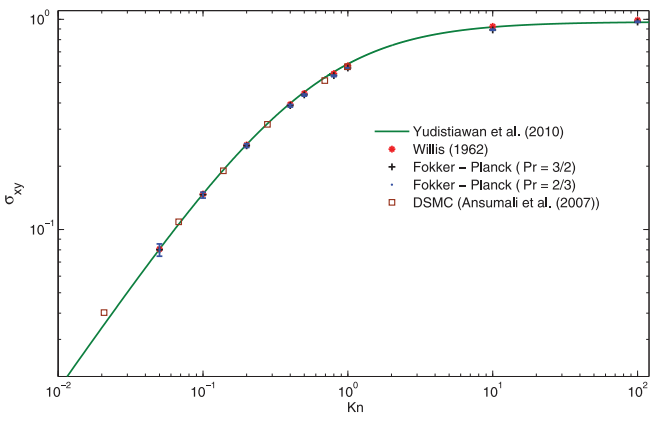

FIG. 3. Shear stress (σ_{xy}) as a function of Kn for Couette flow.

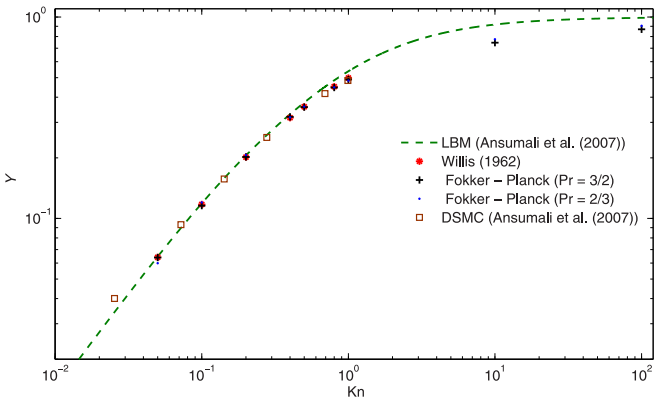

FIG. 4. Difference between the velocity slope at the centerline and its continuum value or Navier-Stokes prediction (Y) with Kn.

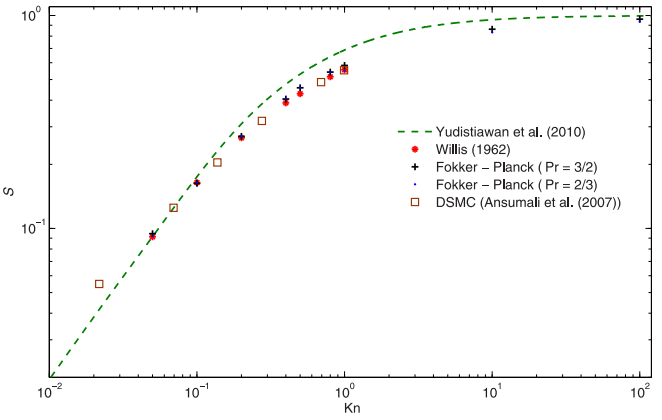

FIG. 5. Velocity slip at the wall (S) with Kn.

values of Kn (shown in Fig. 4). Furthermore, in Fig. 5, velocity slip at the wall obtained via FP simulations is contrasted with that provided in Ref. [35], lattice Boltzmann solution of Ref. [15], and DSMC result [15]. Thus, similar to higher-order LB, regularized 13 moment equation, and DSMC, the present model is also able to predict behavior of Couette flow for finite Knudsen number. Here, it is evident from Figs. 4 and 5 that lattice Boltzmann method fails to capture exact dynamics for Kn $\geqslant 0.25$. Whereas the present FP approach simulates these three quantities correctly in even transitional regime. Finally, it can be also seen that from the results, as expected, different Pr values have no effect on isothermal Couette flow.

B. Poiseuille flow

As second setup, we consider Poiseuille flow in which a pressure/force (F) driven flow between the two infinitely long parallel plates, which are kept at $y = -L/2$ and $y = L/2$, is considered. The physical quantity of interest is often the nondimensional mass flow rate (Q):

$$Q = -\frac{1}{L^2}(F)^{-1}\sqrt{\frac{2k_BT_0}{m}}\int_{-L/2}^{L/2} u_x dy. \tag{48}$$

Like Couette flow, Poiseuille flow problem was also solved using via variational optimization method [36], lattice Boltzmann method [20], and regularized equations [37]. For this extensively studied setup via various analytical and numerical approaches [20,36,37], it is widely agreed that the velocity profile at steady state is of the form

$$u_x(y) = F\frac{y^2}{2\tau} + A_2 + A_3\cosh\left(\frac{y}{c_1 \mathrm{Kn} L}\right), \tag{49}$$

where A_2, A_3, and c_1 are the appropriate model-dependent constants [20,37]. Thus, using Eq. (49) the flow rate can be evaluated as

$$Q = -\frac{1}{6\mathrm{Kn}} + \Gamma_1 + \Gamma_2\mathrm{Kn} - \frac{\Gamma_3 + \Gamma_4\mathrm{Kn} + \Gamma_5\mathrm{Kn}^2}{\Gamma_6\coth\left(\frac{\Gamma_7}{\mathrm{Kn}}\right) + 1}, \tag{50}$$

where $\Gamma_1, \Gamma_2, \ldots$ and Γ_7 are the model-dependent constants [20,37]. Again, we choose to work with the LB model, which shows very good agreement with the true Boltzmann dynamics for the given setup. In particular, for off-lattice $D3Q27$ LB model of Ref. [20], values of A_2, A_3, and c_1 are

$$A_2 = F\tau\left[-2 - \frac{0.25}{\mathrm{Kn}^2} - \frac{1.08152}{\mathrm{Kn}} + \frac{\mathrm{Kn} + 0.165911}{0.970474\mathrm{Kn} + 1.0125\mathrm{Kn}\coth\left(\frac{0.248039}{\mathrm{Kn}}\right)}\right], \tag{51}$$

$$A_3 = F\tau\left[\frac{116.609\mathrm{Kn} + 19.3468}{75.696\mathrm{Kn}\sinh\left(\frac{0.248039}{\mathrm{Kn}}\right) + 78.9739\mathrm{Kn}\cosh\left(\frac{0.248039}{\mathrm{Kn}}\right)}\right], \tag{52}$$

and $c_1 = 2.01581$. For this case, values of $\Gamma_1, \Gamma_2, \ldots$ and Γ_7 are given in the Table I.

In order to simulate the isothermal steady Poiseuille flow using the modified FP approximation for the Boltzmann equation, we have created a computational zone with 200 $\times$ 4 $\times$ 4 cells, where each cell contains 500 gaseous molecules. Diffusive boundary condition was applied on top and bottom walls of channel and periodic boundary condition was applied in other two directions [50]. In this setup of steady Poiseuille flow for gaseous microflow, the nonhydrodynamic behavior is characterized by so-called Knudsen paradox or Knudsen minimum phenomenon. It is known that methods such as LB give only qualitative correct behavior and are quantitatively correct only for Kn < 0.5 only. This behavior was apparent in our simulations too. In Fig. 6, present simulation results are contrasted with the BGK, LB, and DSMC results. Present methodology, similar to Boltzmann-BGK and DSMC, is able

TABLE I. Constants appearing in a generic form for dimensionless flow rate Q in Eq. (50).

LB model	Γ_1	Γ_2	Γ_3	Γ_4	Γ_5	Γ_6	Γ_7
D3Q27	1.08152	2.0	0.17096	2.06084	6.21071	1.04330	0.248039

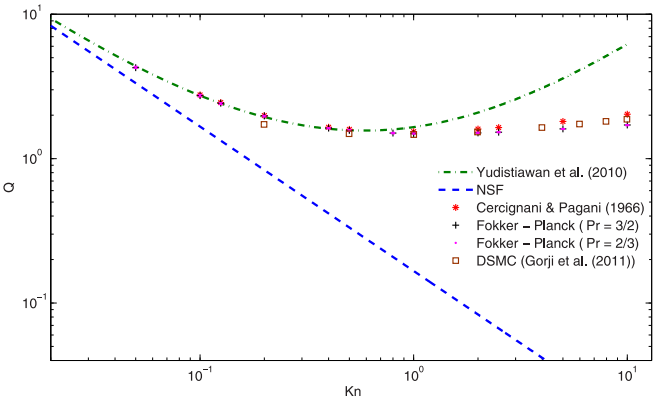

FIG. 6. Mass flux (Q) vs. Knudsen number (Kn) for Poiseuille flow.

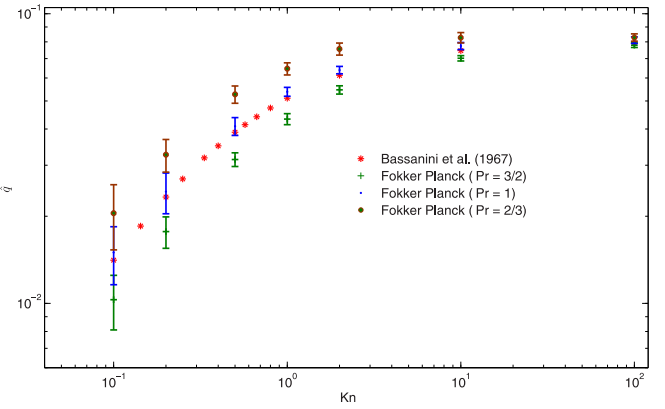

FIG. 7. Heat flux ($\hat{q}$) with Kn for different models.

to predict this phenomena of Knudsen minima in a quantitatively correct fashion. Indeed, it is evident from Fig. 6 that the FP approximation to the Boltzmann equation is quantitatively correct for the transitional region ($0.05 < \mathrm{Kn} < 5$). However, as shown in Fig. 6, similar to any particle method stronger fluctuation for smaller Kn is observed. As expected, in this regime of low Knudsen number, LB provides good results up to $\mathrm{Kn} \approx 0.25$. Thus, present methodology should complement LB for high Knudsen number flows.

C. Heat transfer between parallel plates

Another standard setup for studying the effectiveness of the finite Knudsen flow solvers is the heat transfer between infinitely long parallel plates separated by a distance L. In this setup, the bottom and top plates are kept at different temperatures $T_1(= T - \Delta T)$ and $T_2(= T + \Delta T)$, respectively. The relevant quantity in this setup is the normalized heat flux defined as $\hat{q}(= q/q_{FM})$, where q,q_{FM} are the absolute heat flux and free molecular heat flux, respectively. Thus, this setup can also be used to test ability to tune Prandtl number in simulations. Following [39], q_{FM} can be written as

$$q_{FM} \approx -\frac{\sqrt{2}\zeta}{2-\zeta}\frac{2\Delta T}{\sqrt{\pi}}, \tag{53}$$

where ζ is the accommodation coefficient and assumed to be one for the present study.

Reference [38] derived the approximate value of the normalized heat flux, valid for small temperature difference ($\Delta T \ll 1$), as

$$\hat{q} = \frac{1}{1 + \frac{4}{5\sqrt{\pi}\,\mathrm{Kn}}}. \tag{54}$$

To simulate the heat transfer between the parallel plates, we considered $200 \times 4 \times 4$ cells with each cell containing 500 gaseous particles. The diffusive wall condition was applied on top and bottom walls of channel, while periodic boundary condition was applied in other two directions. In Fig. 7, it is evident that in low Kn regime the magnitude of heat flux increases as Pr decreases, and approximately Fourier's law of heat transfer is captured at $\mathrm{Kn} = 0.05$. Also, It is found that the heat flux is approximately independent of Prandtl number in free molecular regime ($\mathrm{Kn} \to \infty$). Similarly, simulations show stronger fluctuations at low Kn and low Pr. It is also evident from Fig. 7 that FP results for $\mathrm{Pr} = 1$ have good match with BGK based variational solution [38]. It is observed from magnitude of heat flux for different Kn and Pr that the contribution of correction term in free flight of molecule is stronger at high value of Kn and low value of Pr.

D. Normal shock tests

An important canonical test problem for kinetic-theory-based model is that of normal shock wave [40,55–57]. As the Ma increases, departure from equilibrium becomes stronger and thus dynamics of higher-order moments become sensitive to details of the kinetic model being used. Therefore, we do not expect the present simplified collision dynamics to provide quantitative agreement with Boltzmann dynamics in case of highly nonequilibrium flows and we restrict the attention to regime of $\mathrm{Ma} < 2$.

We study one-dimensional normal shock structure in a shock stationary frame of reference. In this problem, a long tube is initially separated into two regions at mid by a thin diaphragm (as shown in Fig. 8). At time $t = 0$, the diaphragm is removed and the two regions of gas are left to interact. The initial conditions for density, velocity, and temperature are specified using the Rankine-Hugoniot conditions [55]. The downstream quantities (ρ_2, u_2, T_2) in terms of upstream quantities (ρ_1, u_1, T_1) can be written as

$$\rho_2 = \frac{\rho_1(\gamma+1)\mathrm{Ma}_1^2}{2+(\gamma-1)\mathrm{Ma}_1^2}, \quad u_2 = \frac{u_1\left(2+(\gamma-1)\mathrm{Ma}_1^2\right)}{(\gamma+1)\mathrm{Ma}_1^2},$$
$$T_2 = \frac{T_1\left(2\gamma\mathrm{Ma}_1^2-(\gamma-1)\right)\left((\gamma-1)\mathrm{Ma}_1^2+2\right)}{(\gamma+1)^2\mathrm{Ma}_1^2}. \tag{55}$$

where γ is the adiabatic exponent and Ma_1 is the upstream Mach number. The discontinuity in the initial condition smooths with time and the shock structure is resolved.

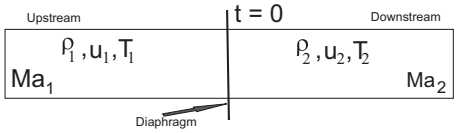

FIG. 8. Schematic diagram for normal shock test.

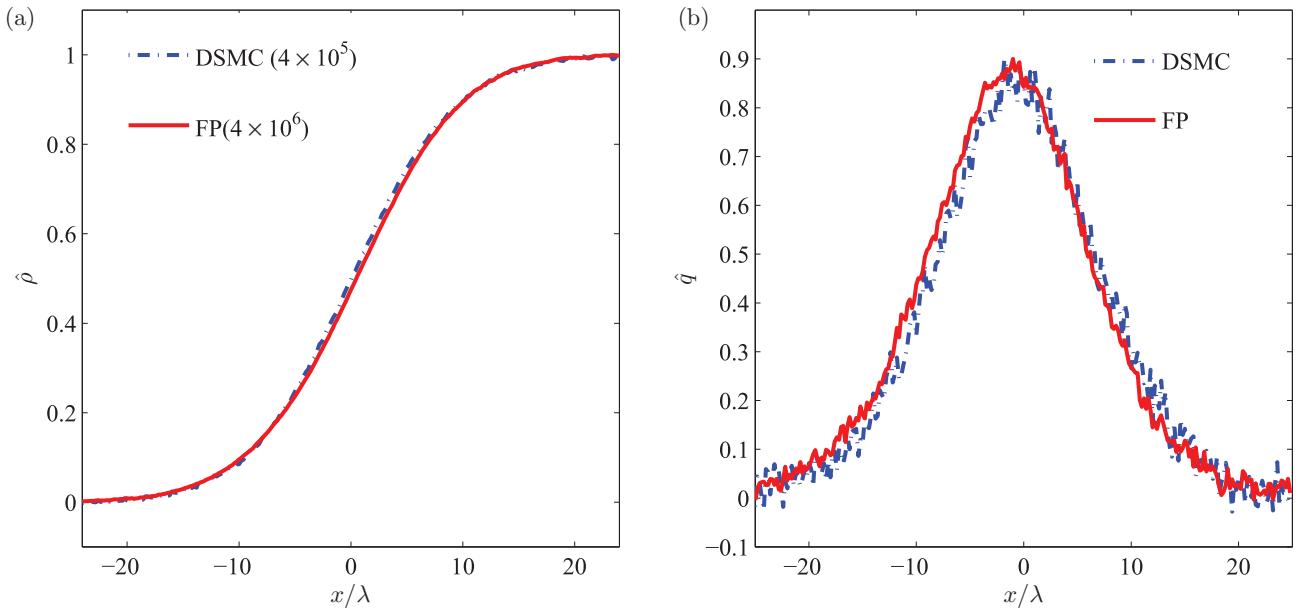

FIG. 9. Normalized density ($\hat{\rho}$) and heat flux ($\hat{q}$) at $\mathrm{Ma}_1 = 1.1$ versus x/λ, where λ is mean-free length. 4×10^5 and 4×10^6 gaseous particles gaseous particles were taken for DSMC and FP simulations, respectively.

To verify computational compatibility and efficiency of present algorithm for supersonic flows, simulations were carried out for different $\mathrm{Ma}_1 = 1.1, 1.5$ and shock structure was resolved for each case. Simulations were carried out with 250 and 300 cells in the shock direction for $\mathrm{Ma}_1 = 1.1$ and $\mathrm{Ma}_1 = 1.5$ cases, respectively, and time averaging was carried out over 200 ensembles in order to calculate macroscopic quantities. In every simulation, supersonic inlet and subsonic outlet boundary conditions was used for both FP and DSMC. In this approach, we used a supersonic inlet condition on the left boundary and a subsonic outlet condition on the right boundary according to Refs. [51,52]. All the variables (ρ, u, T) are imposed on the left boundary, as all the characteristics move into the interior of the domain for a supersonic inlet. For a subsonic outlet, we impose only pressure, as there is only one characteristic moving into the domain from outside, and the rest are calculated from the neighboring boundary cells according to Refs. [51,52]. As the density is proportional to the number of particles in a cell, additional particles are introduced and removed in the boundary cells according to the required density. The boundary cells are completely reinitialized uniformly in space and with Maxwellian distribution in velocity, pertaining to the values obtained at respective boundaries.

Normalized density ($\hat{\rho}$) profile and normalized heat flux ($\hat{q}$) profile based on FP and DSMC simulation results for $\mathrm{Ma}_1 = 1.1$ are plotted in Fig. 9. It can be seen that FP results

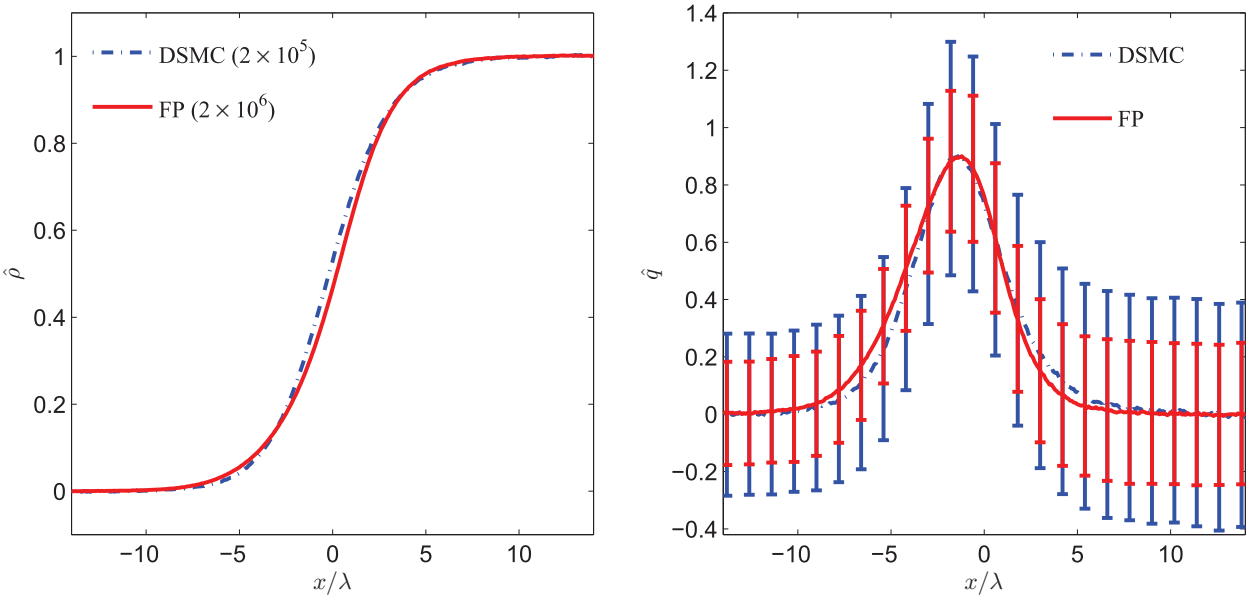

FIG. 10. Normalized density ($\hat{\rho}$) and heat flux ($\hat{q}$) at $\mathrm{Ma}_1 = 1.5$ versus x/λ, where λ is mean-free length. 2×10^5 and 2×10^6 gaseous particles were taken for DSMC and FP simulations, respectively.

closely match with DSMC for $Ma_1 = 1.1$. Though, for same quality results, FP requires roughly one order of magnitude more particles per cell. However, even with order of magnitude more particles, FP simulations are much cheaper than DSMC due to $O(N)$ scaling of FP methods. Here, we remind that the number of particles required for DSMC increase quite drastically and corresponding simulation cost increase as $O(N^2)$ for low Mach number simulations. Thus, FP approach is quite efficient in this case of moderate and also for case of low Mach number simulations. Plots for normalized heat flux ($\hat{q}$) in DSMC and FP confirm that large number of ensembles are required to capture higher-order moments properly.

Similarly, normalized density ($\hat{\rho}$) profile and normalized heat flux ($\hat{q}$) profile based on FP and DSMC simulation results for $Ma_1 = 1.5$ are plotted in and Fig. 10. Even though density profile for FP has good agreement with DSMC, heat flux profiles show differences among two methods. Normalized heat flux plots confirm that the FP approach suffers from stronger fluctuations than DSMC for higher Mach number. In FP approach, increasing the number of particles in computational cell provides only better average, whereas fluctuations (or deviation from average) are inversely proportional to the square root of number of particles. Here, it is important to note that accurate calculation of correction term in advection, which depends on local temperature gradient, for higher Ma requires finer resolution and this term starts dominating over actual molecular velocity, so this approach deviates from DSMC for high Ma number. This result suggests that FP approach should be used only for low Mach number and transonic regime only.

V. OUTLOOK

A FP-based simulation framework was developed and tested for various canonical setups such as Couette flow, Poiseuille flow, and heat flow between infinitely long parallel plates over wide range of Knudsen number. It is found that the present FP approximation to the Boltzmann equation works efficiently for isothermal Couette flow and isothermal Poiseuille flow in transitional regime. In case of heat transfer, effect of Pr is correctly reproduced. Normal shock wave simulation results suggest that FP approach reproduces results of DSMC in transonic flow regime and requires an order of magnitude more particles per cell. However, in low Mach and transonic flow regime, FP-based methods lead to an order of magnitude improvement over DSMC due to the fact that collision in FP does not require sorting steps. Also, it is found that FP approach is more efficient than DSMC in the case of larger system size. To conclude, FP approximation to the Boltzmann equation provides a convenient phenomenological model at single-particle distribution function level with tunable Prandtl number. The results for the canonical flow setups suggest that FP approach is a possible alternate in the low Mach number and transonic regime for simulating hydrodynamics of rarefied gases. Finally, it should be stressed that the current approach of Langevin dynamics has a distinct disadvantage that the momentum and energy conservation laws are valid only on an average.

ACKNOWLEDGMENTS

S. K. Singh expresses his sincere thanks to National Board of Higher Mathematics, DAE, India for their financial support (Grant No. 2/40/14/2012/R&D-II/8128). S. Ansumali expresses his sincere thanks to Department of Science and Technology, India for financial assistance (Grant No. SB2/S2/CMP-056/2013).

[1] E. S. Oran, C. K. Oh, and B. Z. Cybyk, Annu. Rev. Fluid Mech. **30**, 403 (1998).
[2] G. E. M. Karniadakis, A. Beskok, and M. Gad-el Hak, Appl. Mech. Rev. **55**, B76 (2002).
[3] M. C. Bravo, J. Appl. Phys. **102**, 074905 (2007).
[4] J. Kang, N. I. Prasianakis, and J. Mantzaras, Phys. Rev. E **89**, 063310 (2014).
[5] X. Zhang, L. Xiao, X. Shan, and L. Guo, Sci. Rep. **4**, 4843 (2014).
[6] S. Chapman and T. G. Cowling, *The Mathematical Theory Nonuniform Gases* (Cambridge University Press, Cambridge, 1970).
[7] C. Cercignani, *Theory and Application of the Boltzmann Equation* (Scotish Academy Press, Edinburg, 1975).
[8] F. J. Alexander, A. L. Garcia, and B. J. Alder, Phys. Fluids **6**, 3854 (1994).
[9] A. Beskok and G. E. M. Karniadakis, Microscale Therm. Eng. **3**, 43 (1999).
[10] Y. Zheng, A. L. Garcia, and B. Alder, J. Stat. Phys. **109**, 495 (2002).
[11] S. Ansumali and I. V. Karlin, Phys. Rev. E **66**, 026311 (2002).
[12] F. Toschi and S. Succi, Europhys. Lett. **69**, 549 (2005).
[13] M. Mauro and S. Succi, Phys. Fluids **17**, 093602 (2005).
[14] S. Ansumali, I. Karlin, C. E. Frouzakis, and K. B. Boulouchos, Phys. A **359**, 289 (2006).
[15] S. Ansumali, I. V. Karlin, S. Arcidiacono, A. Abbas, and N. I. Prasianakis, Phys. Rev. Lett. **98**, 124502 (2007).
[16] W. P. Yudistiawan, S. Ansumali, and I. V. Karlin, Phys. Rev. E **78**, 016705 (2008).
[17] S. H. Kim, H. Pitsch, and I. D. Boyd, J. Comput. Phys. **227**, 8655 (2008).
[18] S. H. Kim, H. Pitsch, and I. D. Boyd, Phys. Rev. E **77**, 026704 (2008).
[19] G. H. Tang, Y. H. Zhang, and D. R. Emerson, Phys. Rev. E **77**, 046701 (2008).
[20] W. P. Yudistiawan, S. K. Kwak, D. V. Patil, and S. Ansumali, Phys. Rev. E **82**, 046701 (2010).
[21] N. Prasianakis and S. Ansumali, Commun. Comput. Phys. **9**, 1128 (2011).
[22] V. E. Ambruş and V. Sofonea, Phys. Rev. E **86**, 016708 (2012).
[23] Y. Shi, Y. W. Yap, and J. E. Sader, Phys. Rev. E **89**, 033305 (2014).
[24] V. E. Ambruş and V. Sofonea, Phys. Rev. E **89**, 041301 (2014).

[25] Y. Shi, P. L. Brookes, Y. W. Yap, and J. E. Sader, Phys. Rev. E **83**, 045701 (2011).
[26] J. E. Broadwell, J. Fluid Mech. **19**, 401 (1964).
[27] R. Yano, K. Suzuki, and H. Kuroda, Phys. Fluids **21**, 047104 (2009).
[28] P. Jenny, M. Torrilhon, and S. Heinz, J. Comput. Phys. **229**, 1077 (2010).
[29] M. H. Gorji, M. Torrilhon, and P. Jenny, J. Fluid Mech. **680**, 574 (2011).
[30] C. W. Gardiner, *Stochastic Methods* (Springer-Verlag, Berlin/Heidelberg/New York/Tokyo, 1985).
[31] H. C. Öttinger, *Stochastic Processes in Polymeric Fluids: Tools and Examples for Developing Simulation Algorithms*, Vol. 1 (Springer, Berlin, 1996).
[32] J. L. Lebowitz, H. L. Frisch, and E. Helfand, Phys. Fluids **3**, 325 (1960).
[33] P. L. Bhatnagar, E. P. Gross, and M. Krook, Phys. Rev. **94**, 511 (1954).
[34] S. K. Singh and S. Ansumali, Phys. Rev. E **91**, 033303 (2015).
[35] D. R. Willis, Phys. Fluids **5**, 127 (1962).
[36] C. Cercignani and C. D. Pagani, Phys. Fluids **9**, 1167 (1966).
[37] H. Struchtrup and M. Torrilhon, Phys. Rev. Lett. **99**, 014502 (2007).
[38] P. Bassanini, C. Cercignani, and C. D. Pagani, Int. J. Heat Mass Transfer **10**, 447 (1967).
[39] I. A. Graur and A. P. Polikarpov, Heat Mass Transfer **46**, 237 (2009).
[40] H. W. Liepmann, R. Narashima, and M. T. Chahine, Phys. Fluids **5**, 1313 (1962).
[41] L. H. Holway, Phys. Fluids **9**, 1658 (1966).
[42] S. Heinz, Phys. Rev. E **70**, 036308 (2004).
[43] M. H. Gorji and P. Jenny, Phys. Fluid **25**, 062002 (2013).
[44] M. H. Gorji and P. Jenny, J. Comput. Phys. **262**, 325 (2014).
[45] M. H. Gorji and P. Jenny, J. Comput. Phys. **287**, 110 (2015).
[46] P. J. M. H. Gorji and N. Andric, J. Comput. Phys. **295**, 644 (2015).
[47] S. Ansumali, Commun. Comput. Phys. **9**, 1106 (2011).
[48] H. Risken, *The Fokker-Planck Equation : Methods of Solution and Applications* (Springer, Berlin, 1986).
[49] T. Ladd, *Lectures at the 3rd Warsaw School of Statistical Physics* (Kazimierz, Poland, 2009).
[50] F. J. Alexander and A. L. Garcia, Comput. Phys. **11**, 588 (1997).
[51] K. W. Thompson, J. Comput. Phys. **89**, 439 (1990).
[52] T. J. Poinsot and S. K. Lele, J. Comput. Phys. **101**, 104 (1992).
[53] M. A. Gallis, T. P. Koehler, J. R. Torczynski, and S. J. Plimpton, Phys. Fluids **27**, 084105 (2015).
[54] D. Wolfe, A. Larraza, and A. Garcia, Phys. Fluids **28**, 037103 (2016).
[55] R. Courant and K. O. Friedrichs, *Supersonic Flows and Shock Waves* (Interscience, New York, 1948).
[56] M. Torrelhon and H. Struchtrup, J. Fluid Mech. **513**, 171 (2004).
[57] G. Bird, *Molecular Gas Dynamics and the Direct Simulations of the Gases* (Oxford University Press, Oxford, 1994).